Advanced Functional Materials 28.5 31 (2018): 1704040
DOI: https://doi.org/10.1002/adfm.201704040

Supporting Information

Reversible thermochromic polymeric thin-films made of ultrathin two-dimensional crystals of coordination polymers based on copper(I)-thiophenolates

Javier Troyano, Oscar Castillo, José I. Martínez, Vanesa Fernández-Moreira, Yolanda Ballesteros, Daniel Maspoch, Félix Zamora,* and Salome Delgado**

Table S1. Crystallographic data for bis-*p*-methoxycarbonyl-phenydisulfide.

	bis-*p*-methoxycarbonyl-phenydisulfide
Empirical formula	$C_{16}H_{14}O_4S2$
Formula weight	334.39
T (K)	296(2)
Crystal system	Triclinic
Space group	*P -1*
a (Å)	5.9491(2)
b (Å)	7.7335(2)
c (Å)	18.0739(5)
α (º)	78.850(2)
β (°)	86.349(2)
γ (°)	75.441(2)
V (Å^3)	789.54(4)
Z	2
GOF[a]	1.028
R_{int}	0.0331
Final R indices [I>2σ(I)]	
R1[b]	0.0353
wR2[c]	0.0808
All data	
R1[b]	0.0603
wR2[c]	0.0911
Largest peak/hole (e$^-$ Å^3)	0.170/-0.184

[a] $S = [\sum w(F_0^2 - F_c^2)^2 / (N_{obs} - N_{param})]^{1/2}$ [b] $R1 = \sum||F_0|-|F_c|| / \sum|F_0|$; [c] $wR2 = [\sum w(F_0^2 - F_c^2)^2 / \sum wF_0^2]^{1/2}$; $w = 1/[\sigma^2(F_0^2) + (aP)^2 + b]$ where $P = (\max(F_0^2,0) + 2F_c^2)/3$ with a = 0.0376 and b = 0.1886.

Table S2. Crystallographic data for compounds **1** and **2** at 110 and 296 K.

	1_{110K}	**1_{296K}**	**2_{110K}**	**2_{296K}**
Empirical formula	$C_7H_5CuO_2S$	$C_7H_5CuO_2S$	$C_8H_7CuO_2S$	$C_8H_7CuO_2S$
Formula weight	216.71	216.71	230.74	230.74
T (K)	110(2)	296(2)	110(2)	296(2)
Crystal system	Orthorhombic	Orthorhombic	Monoclinic	Monoclinic
Space group	*P bca*	*P bca*	*P n*	*P n*
a (Å)	6.8485(6)	6.8406(4)	3.9552(3)	3.9602(12)
b (Å)	5.7083(6)	5.7192(3)	19.0468(16)	19.026(6)
c (Å)	33.959(4)	34.028(2)	5.2605(4)	5.2746(17)
β (°)	--	--	93.184(4)	93.343(16)
V (Å^3)	1327.57(14)	1331.27(14)	395.68(5)	396.7(2)
Z	8	8	2	2
GOF[a]	1.110	1.026	1.076	1.052
R_{int}	0.0343	0.0388	0.0229	0.0243
Final R indices [I>2σ(I)]				
R1[b]	0.0342	0.0298	0.0191	0.0185
wR2[c]	0.0632	0.0541	0.0457	0.0448
All data				
R1[b]	0.0600	0.0486	0.0201	0.0194
wR2[c]	0.0702	0.0588	0.0461	0.0453
Largest peak/hole (e$^-$ Å^3)	0.512/-0.440	0.353/-0.354	0.332/-0.295	0.251/-0.166

[a] $S = [\sum w(F_0^2 - F_c^2)^2 / (N_{obs} - N_{param})]^{1/2}$ [b] $R1 = \sum||F_0|-|F_c|| / \sum|F_0|$; [c] $wR2 = [\sum w(F_0^2 - F_c^2)^2 / \sum wF_0^2]^{1/2}$; $w = 1/[\sigma^2(F_0^2) + (aP)^2 + b]$ where $P = (\max(F_0^2,0) + 2F_c^2)/3$ with a = 0.0214 (**1**), 0.0317 (**2_{110K}**), 0.0311 (**2_{296K}**) and b = 2.1828 (**1**), 0.0095 (**2_{110K}**).

Table S3. Crystal data and selected bonds and angles of **1** at 110 and 296 K.

	Cu-S	Cu···Cu	S-Cu-S	Cu-S-Cu	Cell parameters	V (Å^3)
1 (110 K)	2.243 2.293 2.297	2.992 3.516 3.894	103.61 126.29 129.96	82.45 101.62 116.09	**a**= 6.848 **b**= 5.708 **c=** 33.959	1327.57
1 (296 K)	2.241 2.293 2.304	2.997 3.512 3.897	103.69 126.35 129.83	82.49 101.52 115.95	**a**= 6.841 **b**= 5.719 **c=** 34.028	1331.27

Table S4. Crystal data and selected bonds and angles of **2** at 110 and 296 K.

	Cu-S	Cu···Cu	S-Cu-S	Cu-S-Cu	Cell parameters	V (Å^3)
2 (110 K)	2.239 2.252 2.276	3.305 3.475 3.955	114.24 122.16 123.46	123.46 100.66 93.75	**a**= 3.9552 **b**= 19.0468 **c=** 5.2605	395.68
2 (296 K)	2.239 2.254 2.274	3.305 3.485 3.960	113.95 122.32 123.60	123.60 101.07 93.76	**a**= 3.9602 **b**= 19.026 **c=** 5.2746	396.7

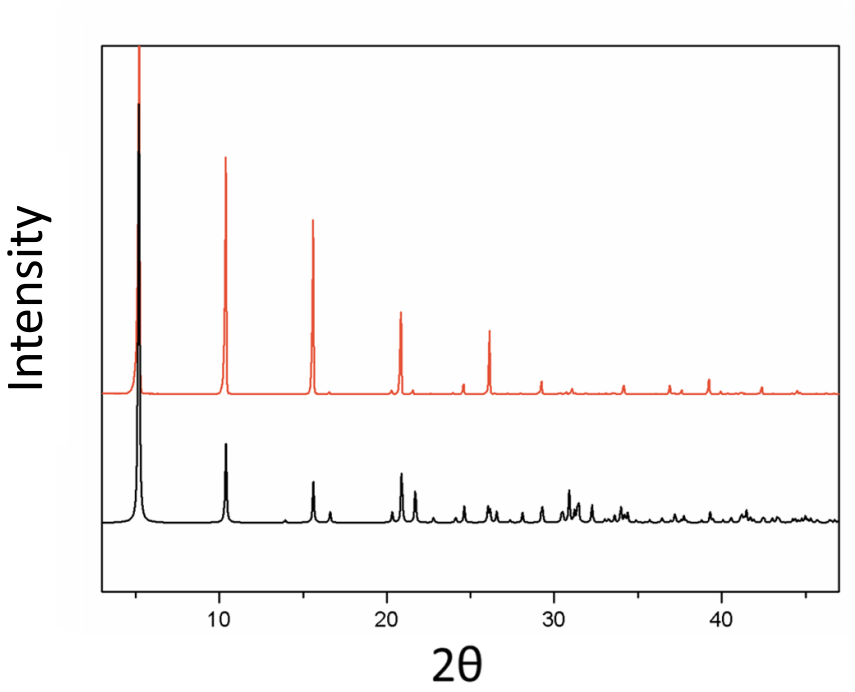

Figure S1. Experimental (red) and simulated (black) XRPD patterns of **1**.

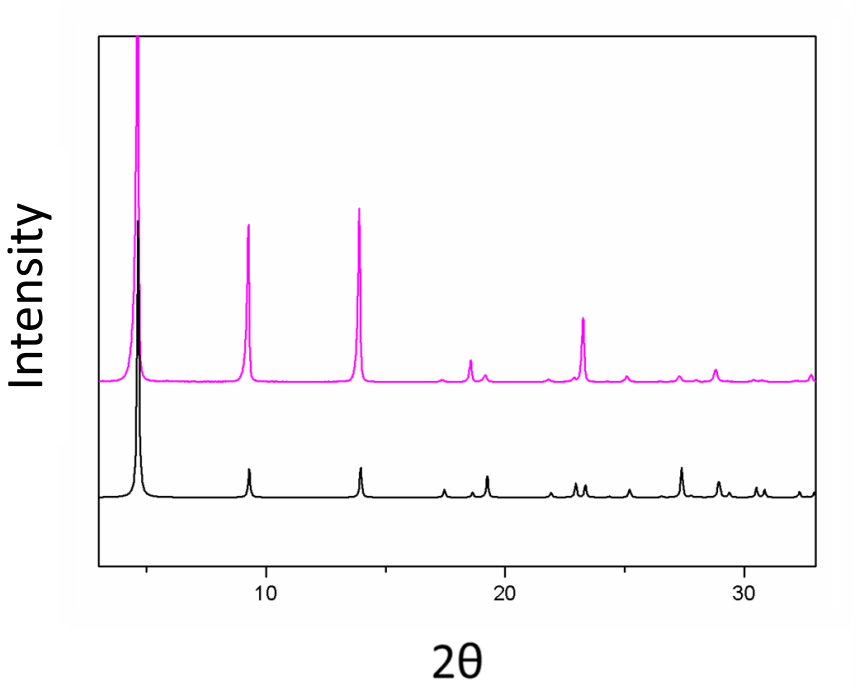

Figure S2. Experimental (pink) and simulated (black) XRPD patterns of **2**.

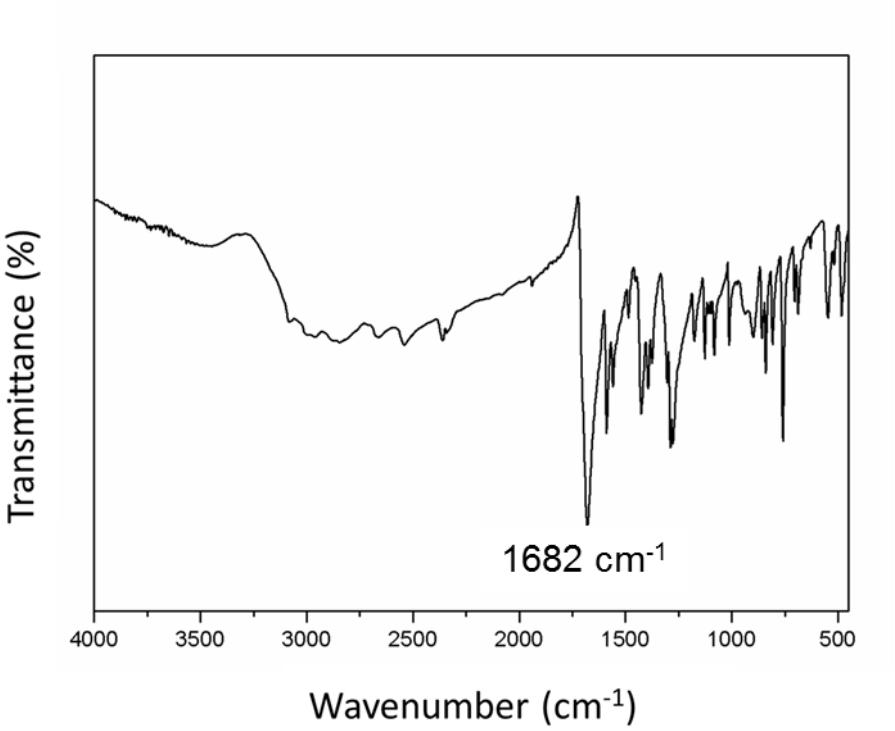

Figure S3. FT-IR spectrum of polycrystalline solid sample of **1** in a KBr pellet.

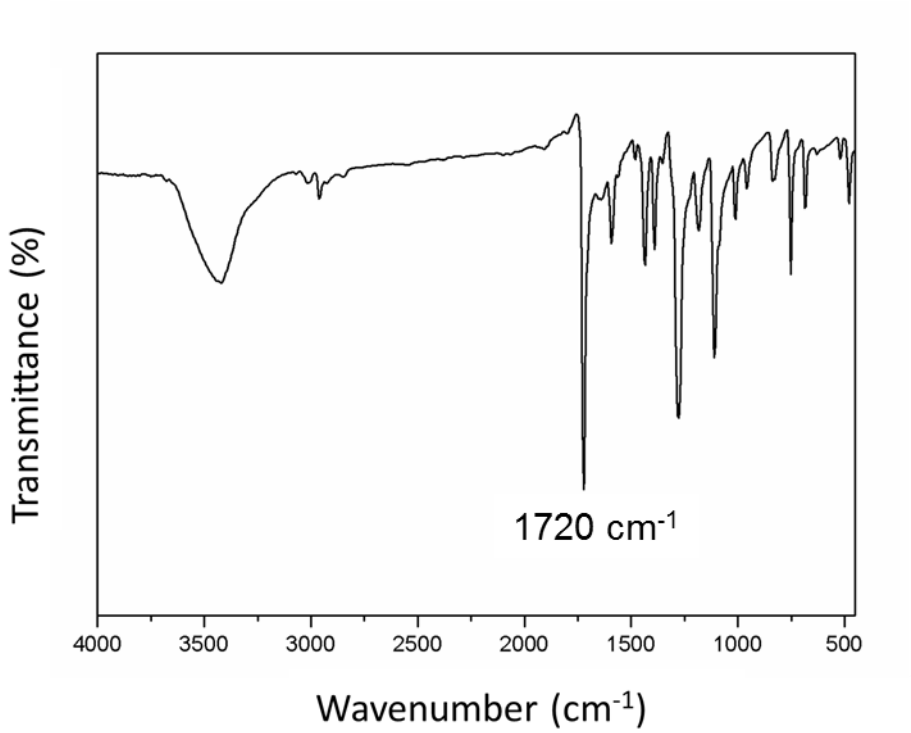

Figure S4. FT-IR spectrum of polycrystalline solid sample of **2** in a KBr pellet.

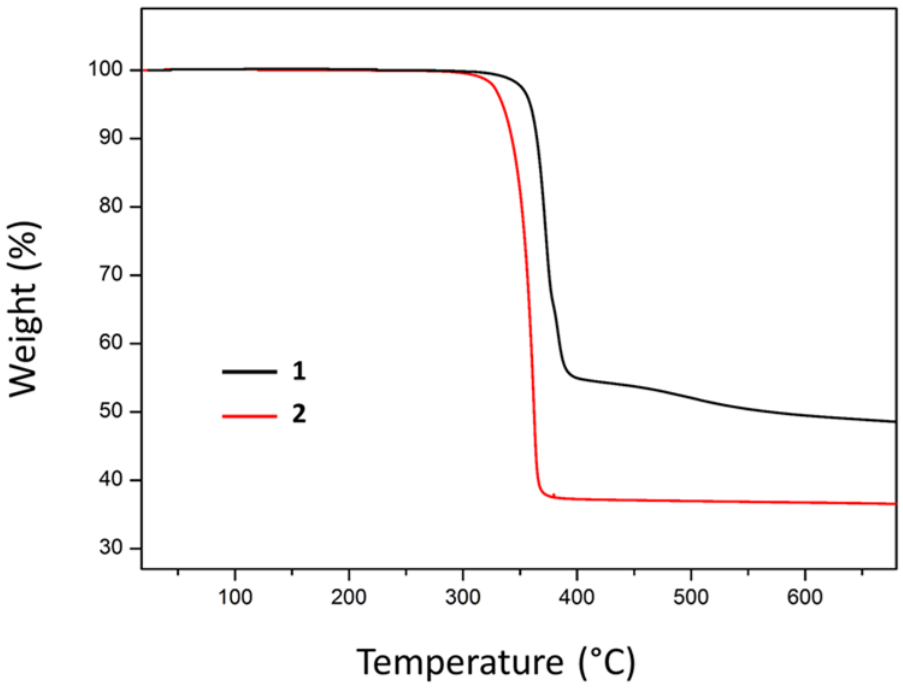

Figure S5. TGA curves of **1** and **2** in N_2 atmosphere.

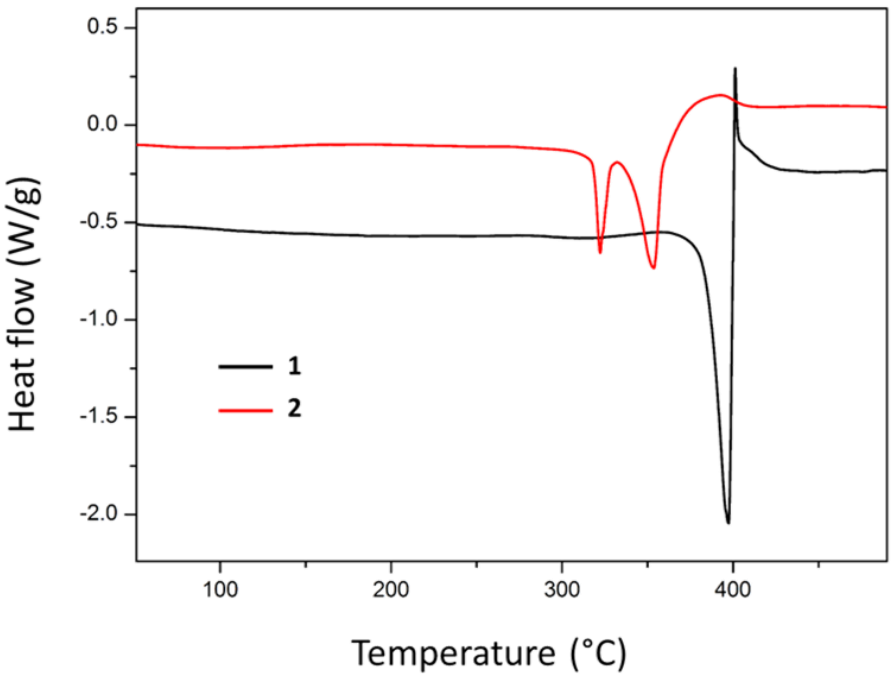

Figure S6. DSC curves of **1** and **2** in N_2 atmosphere.

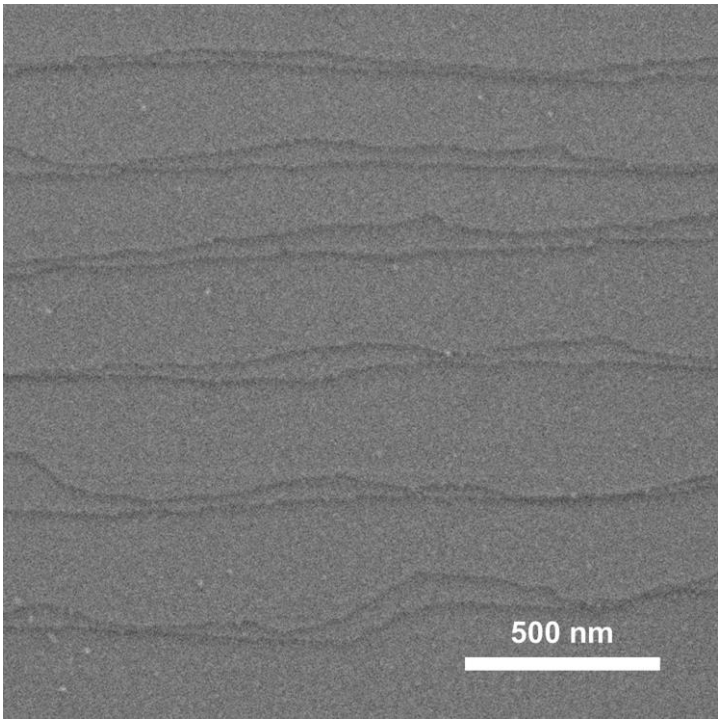

Figure S7. FESEM high-magnification detail of the surface of an individual crystal of **1**.

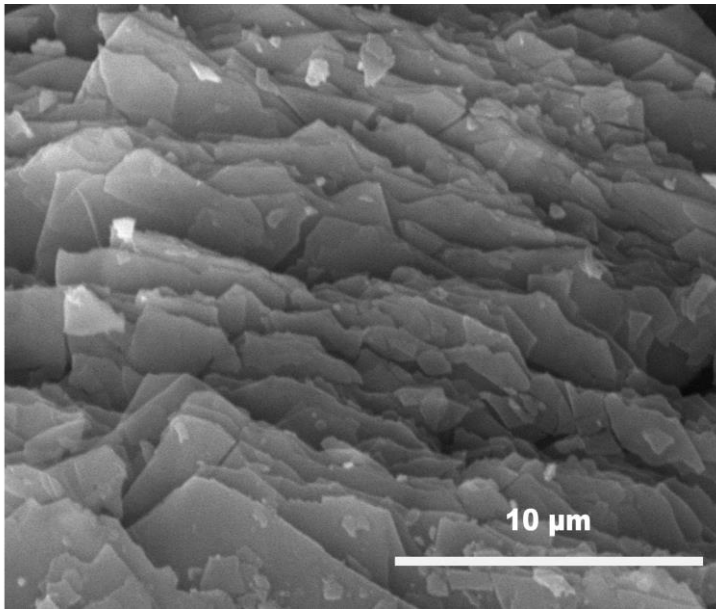

Figure S8. FESEM micrograph of synthesized plate-like microcrystals of $[CuHT]_n$.

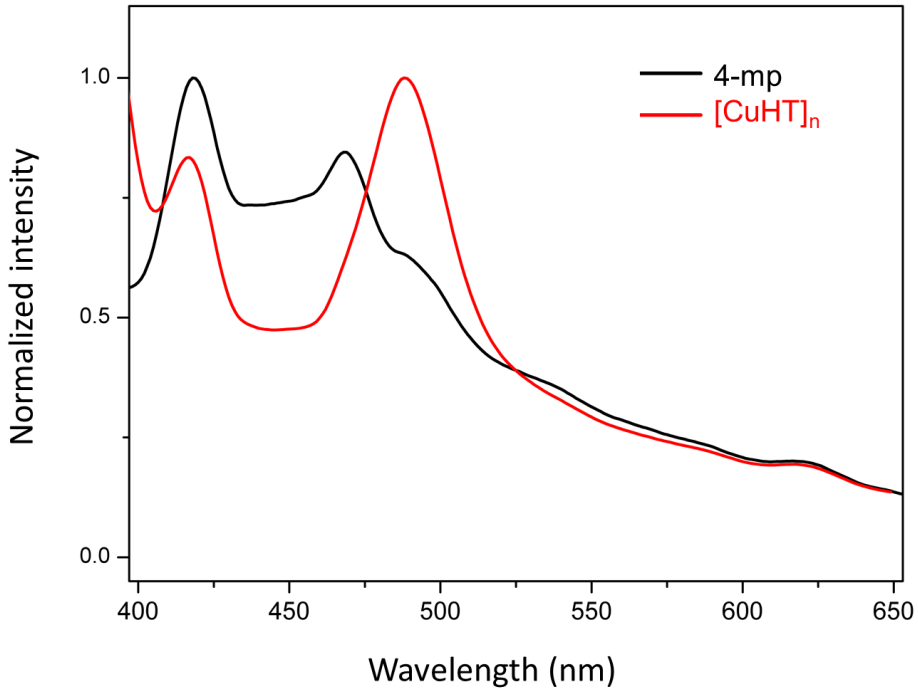

Figure S9. Normalized emission spectra of 4-mercaptophenol (black) and $[CuHT]_n$ (red) in the solid state at room temperature (λ_{exc} = 359 nm).

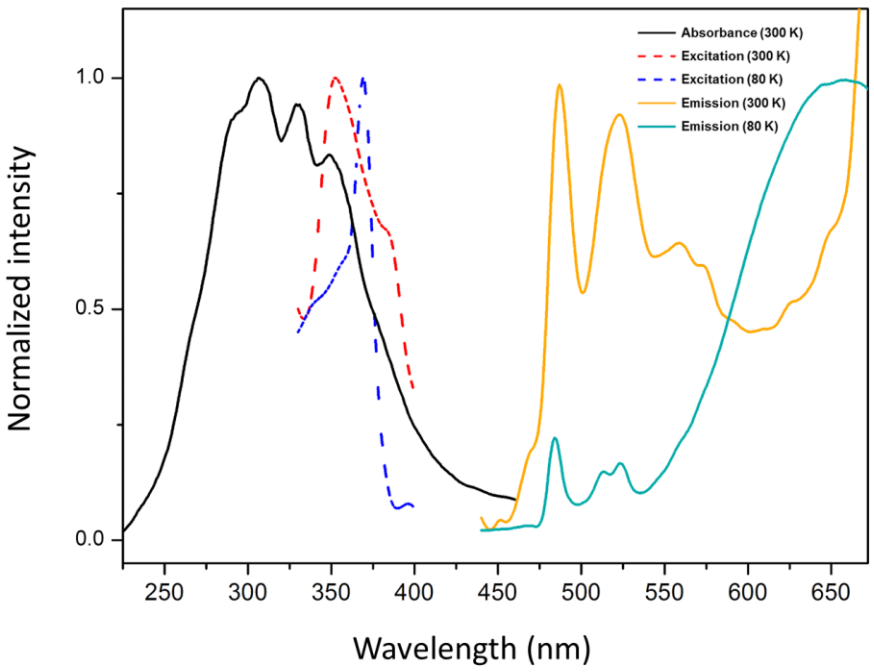

Figure S10. Normalized absorption spectrum at 300 K and excitation (λ_{em} = 484 nm) and emission (λ_{exc} = 350 nm) spectra at 300 and 80 K of **1**.

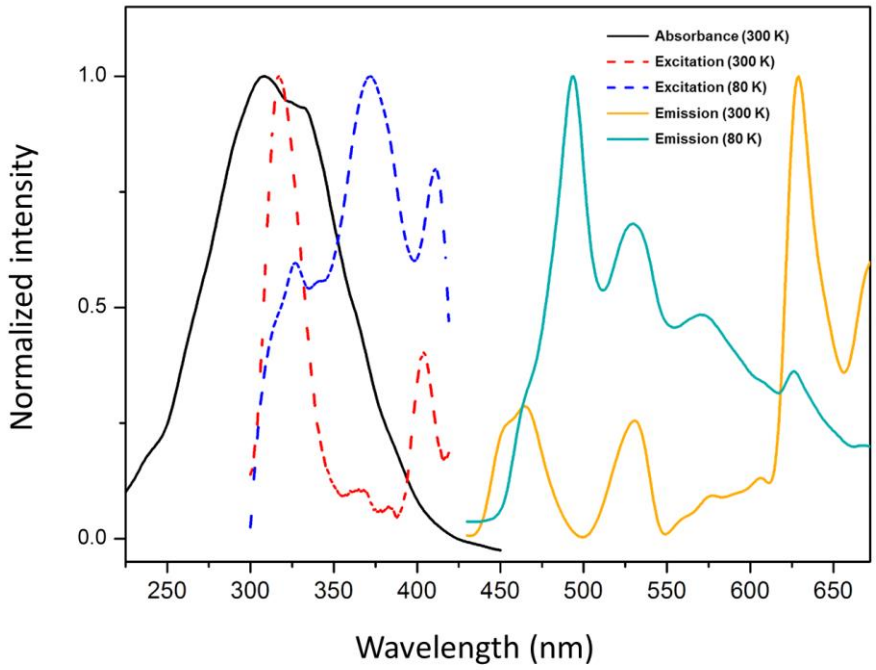

Figure S11. Normalized absorption spectrum at 300 K and excitation (λ_{em} = 500 nm) and emission (λ_{exc} = 350 nm) spectra at 300 and 80 K of **2**.

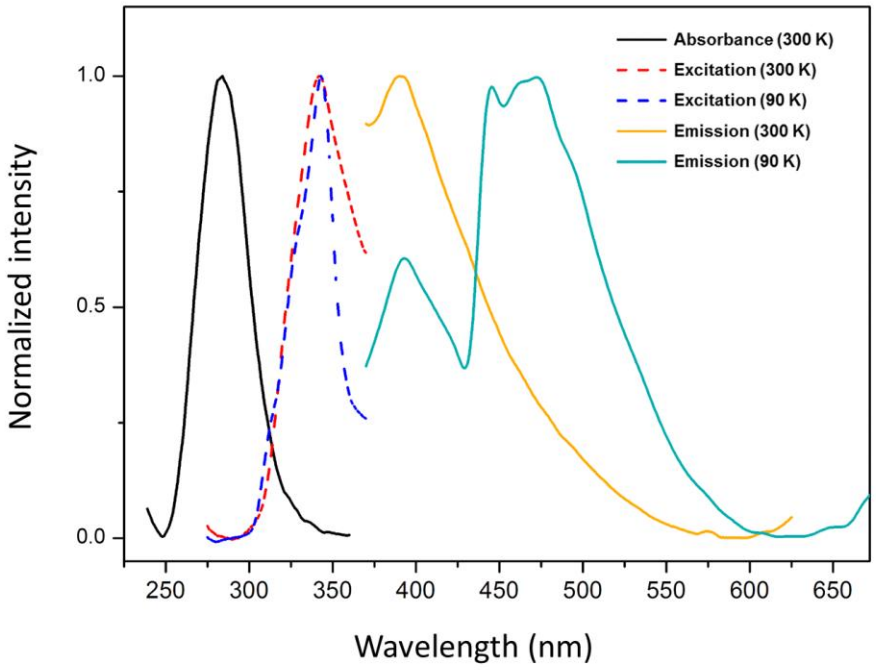

Figure S12. Normalized absorption spectrum at 300 K and excitation (λ_{em} = 390 nm) and emission (λ_{exc} = 350 nm) spectra at 300 and 90 K of 4-mercaptobenzoic acid (4-mba).

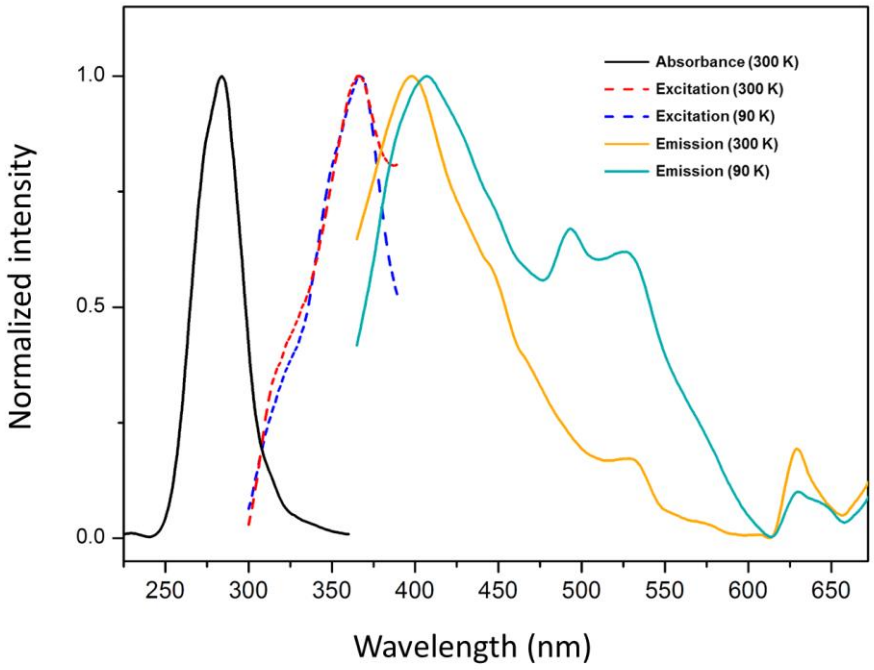

Figure S13. Normalized absorption spectrum at 300 K and excitation (λ_{em} = 411 nm) and emission (λ_{exc} = 350 nm) spectra at 300 and 90 K of 4-mercaptometoxibenzoate (4-mmb).

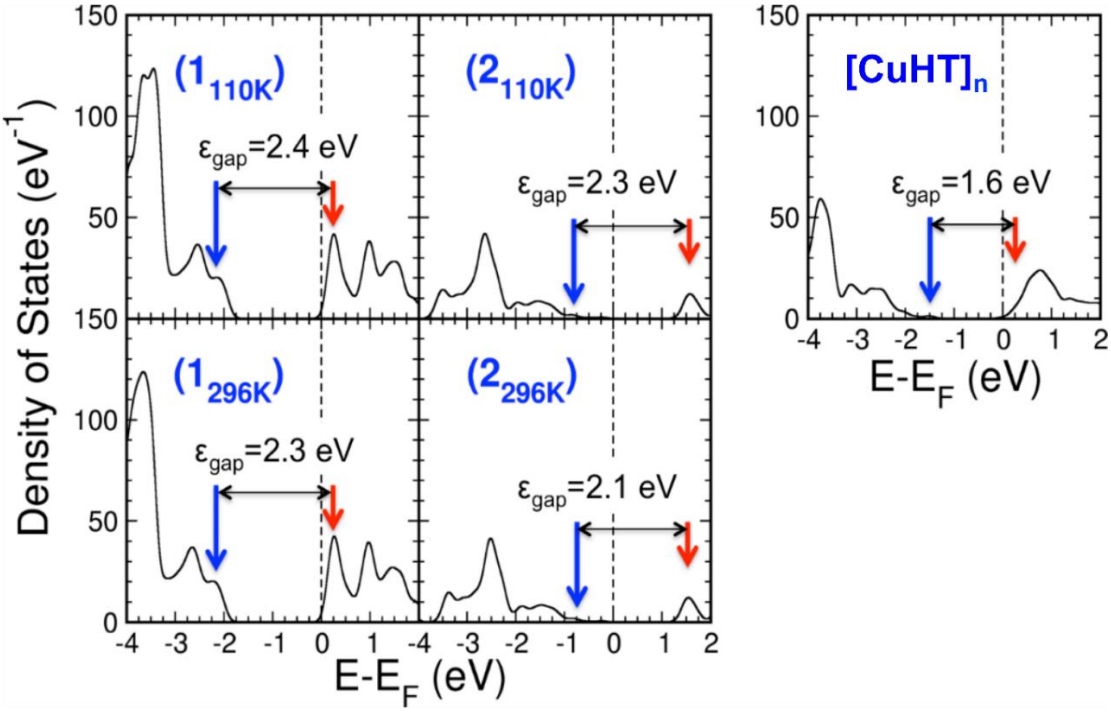

Figure S14. Calculated density of electronic states (in eV^{-1}) for the coordination polymers **1** (**1_{110K}** and **1_{296K}**), **2** (**2_{110K}** and **2_{296K}**) and $[CuHT]_n$ as a function of the energy, referred to the Fermi level. Each energy level has been broadened with by a Lorentzian profile with a line-width of 0.05 eV. Valence and conduction bands for the compounds are indicated by blue and red arrows, respectively, as well as the resulting transport gap is also shown in each subpanel.

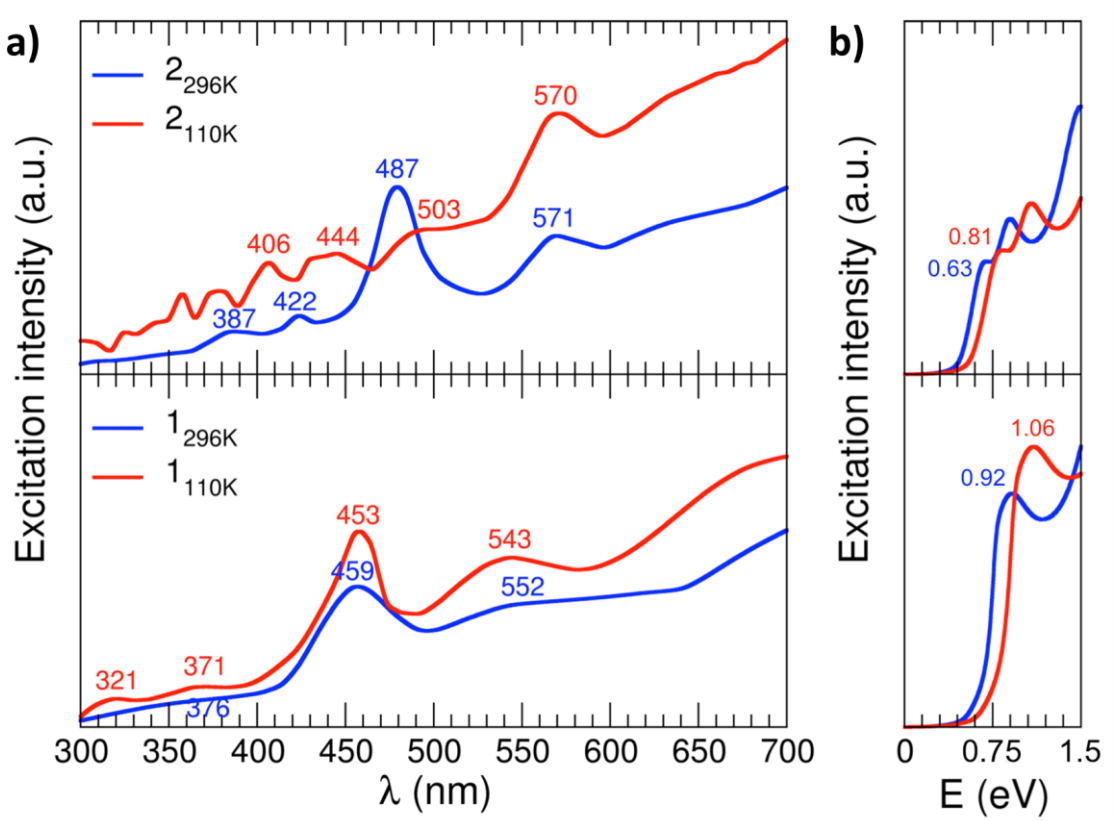

Figure S15. a) Excitation spectra as a function of λ (in nm) computed for compounds **1** and **2** and for both low (110 K; red lines) and high (296 K; blue lines) temperature structures. The wavelength values of the most important transitions for each case have been included. b) Excitation spectra as a function of the excitation energy (in eV) computed for compounds **1** and **2** for both low (110 K; red lines) and high (296 K; blue lines) temperature structures.

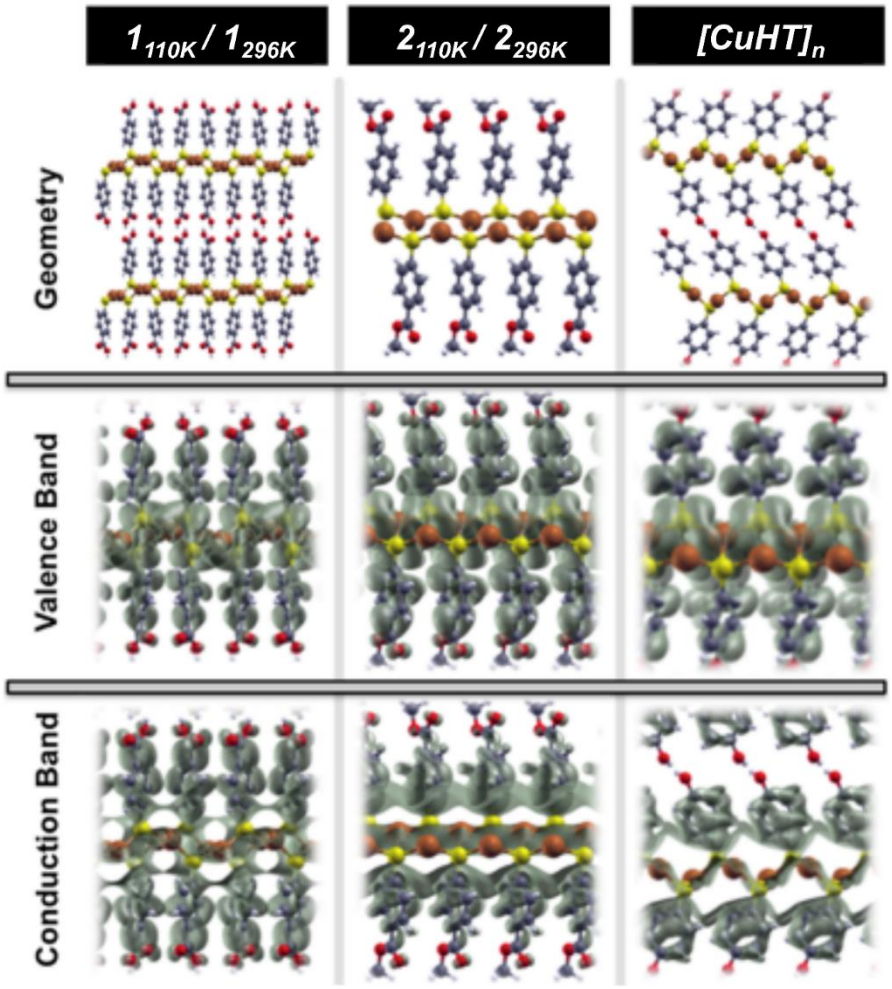

Figure S16. Computed valence (middle panels) and conduction (bottom panels) band orbital electron isodensities (all with a value of 10^{-4} $e^{-}Å^{-3}$) for compounds **1** (for both $\mathbf{1_{110K}}$ and $\mathbf{1}_{296K}$ isodensities are very similar), **2** (for both $\mathbf{2_{110K}}$ and $\mathbf{2_{296K}}$ isodensities are very similar) and for $[CuHT]_n$. Clean geometries are also shown (top panels) for a better comparison.

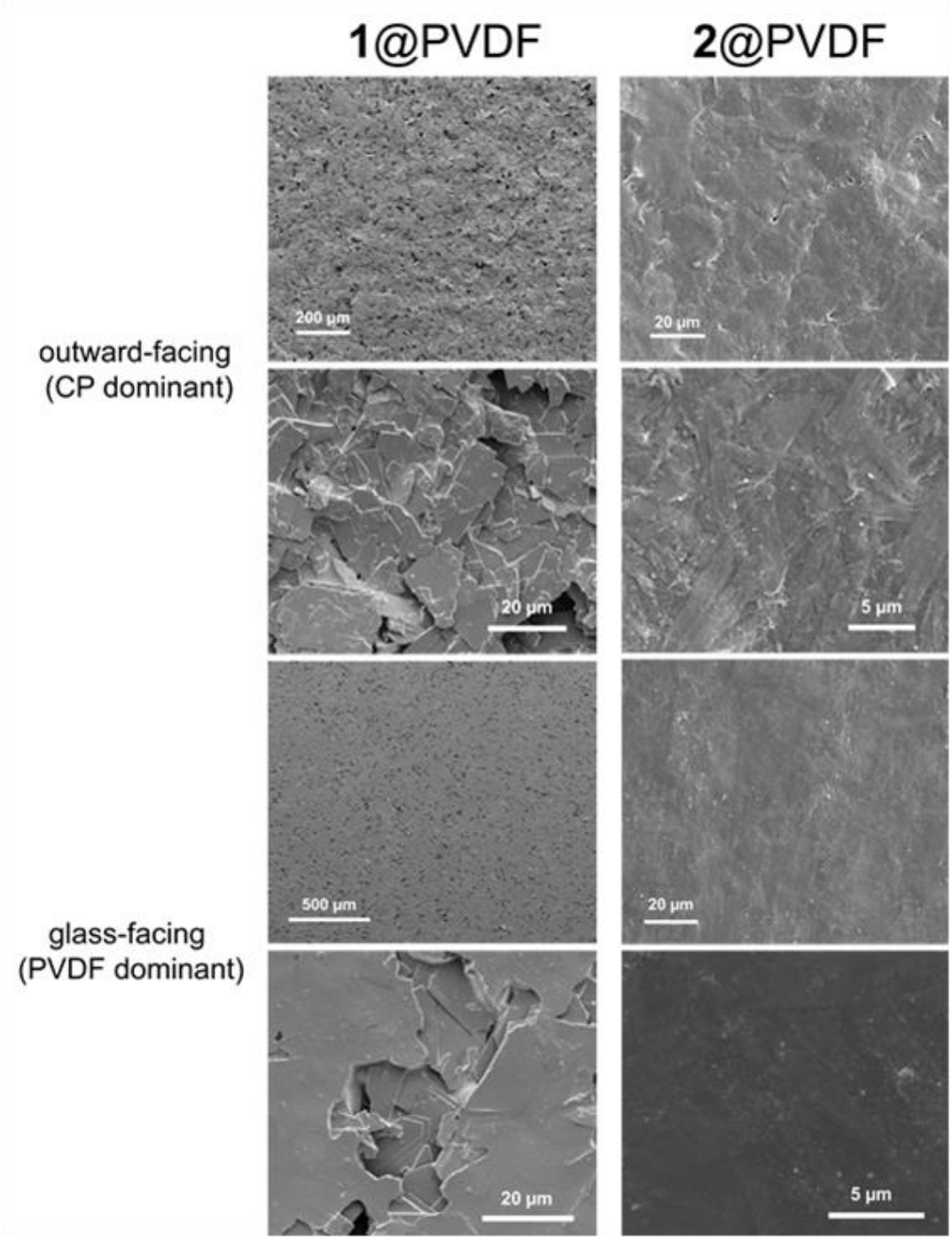

Figure S17. FESEM images of **1**@PVDF (left) and **2**@PVDF (right) with a 50% (wt %) of **1** and **2**, respectively.

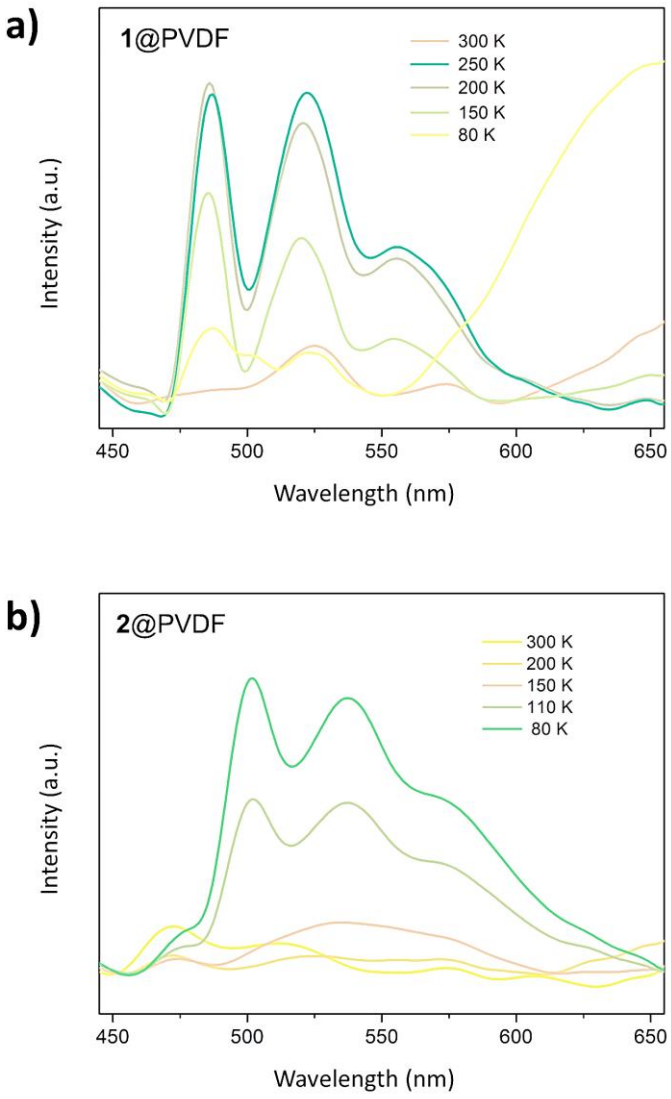

Figure S18. Temperature-dependent luminescence spectra of **1**@PVDF (a) and **2**@PVDF (b) [with a 50% (wt%) of **1** and **2**] from 300 K down to 80 K in the solid state (λ_{exc} = 350 nm).

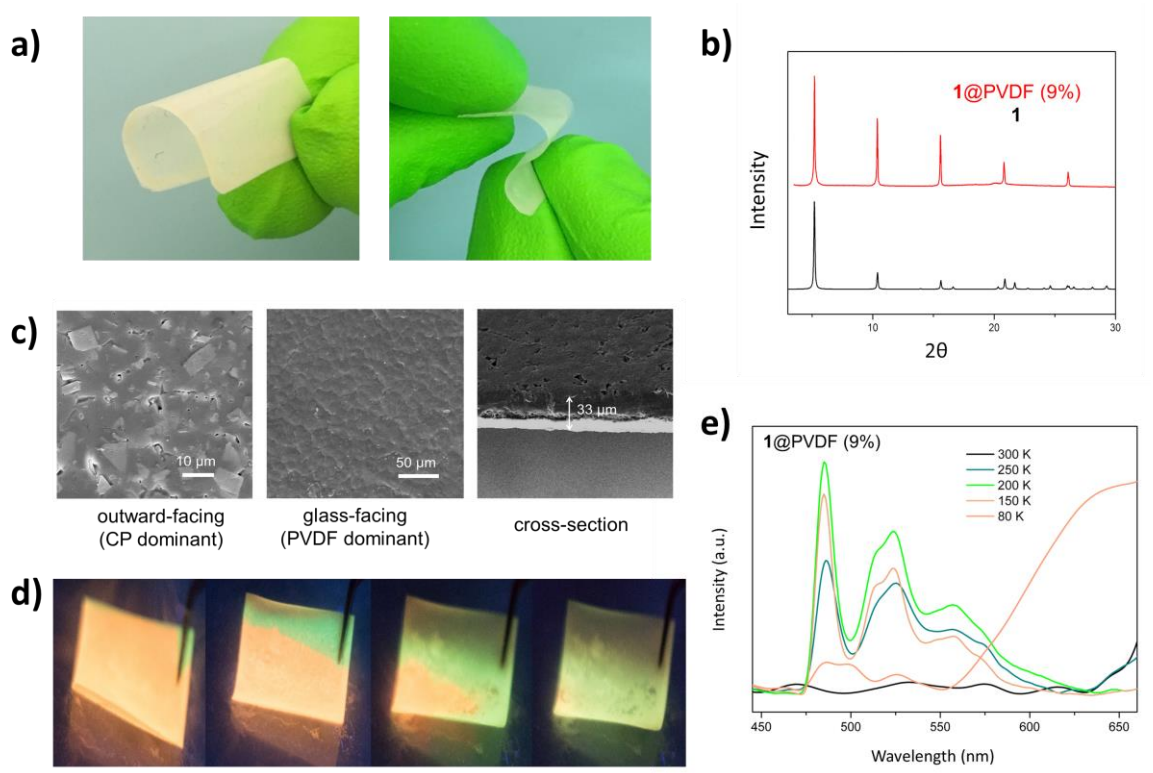

Figure S19. Characterization of prepared **1**@PVDF thin film with a 9 wt% CP content. a) Different photographs of **1**@PVDF (9 wt%) thin film showing its resistance to mechanical stress. b) XRD patterns of **1**@PVDF (9 wt%) thin film and polycrystalline **1**. c) FESEM images of the both sides and the edge view of the **1**@PVDF (9 wt%) thin film. d) Sequential pictures of **1**@PVDF (9 wt%) thin film during warming from 77 K to room temperature under UV lamp excitation (λ_{exc} = 365 nm). e) Temperature-dependent luminescence spectra of **1**@PVDF (9 wt%) from 300 K down to 80 K in the solid state (λ_{exc} = 350 nm).

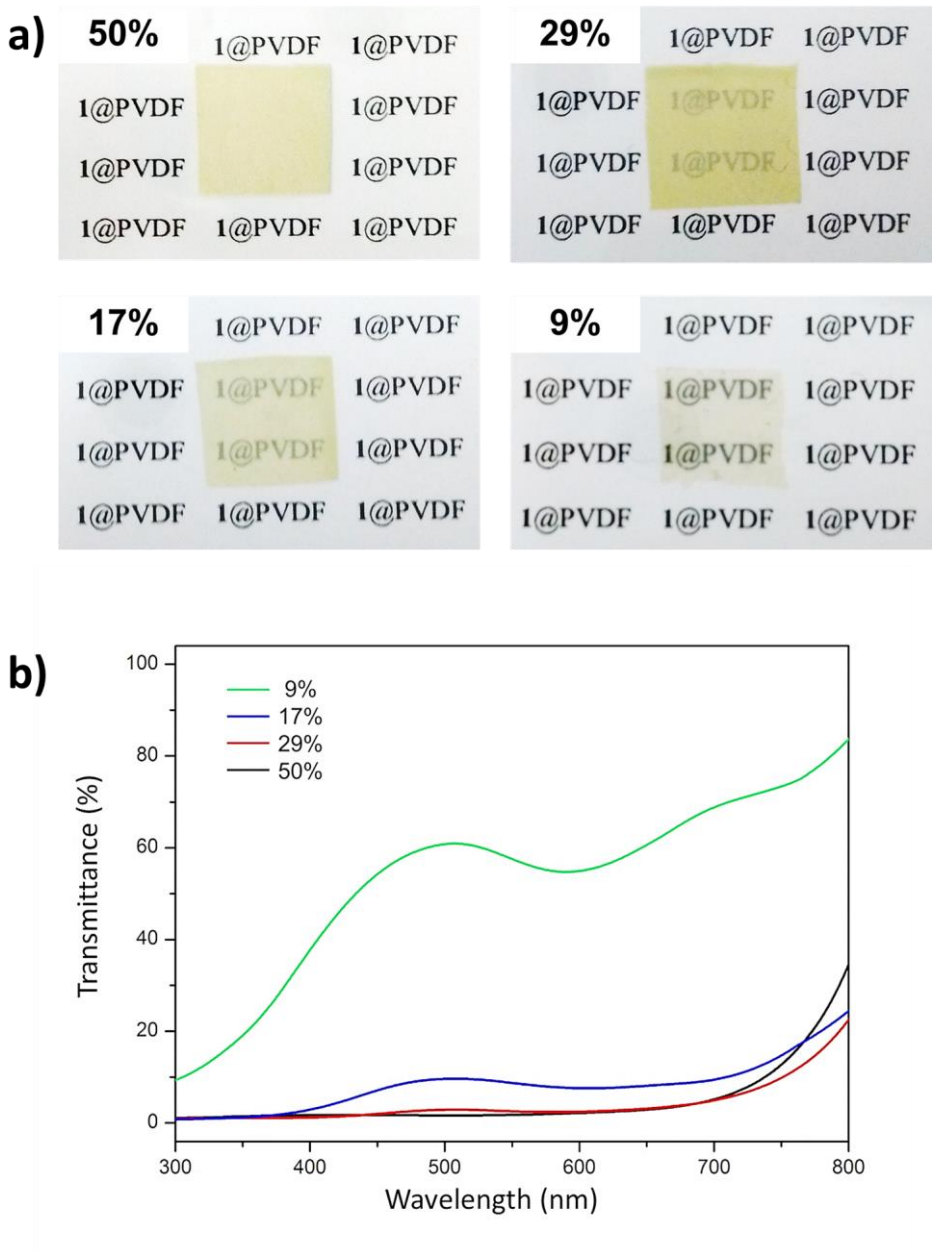

Figure S20. Photographs (a) and optical transmittance (b) of **1**@PVDF thin films with CP content ranging from 9 to 50 wt%.

Table S5. UTS (MPa), E (MPa) and elongation (%) values obtained for naked PVDF film and film composites of **1@PVDF** and **2@PVDF** at 9 and 50 wt%.

Sample	UTS (MPa)	E (MPa)	Elongation (%)
PVDF	8.1±0.1	151±29	12.3±2.4
1@PVDF 9 % (wt %)	8.1±0.6	194±38	8.2±0.4
1@PVDF 50 % (wt %)	1.5±0.8	71±34	6.0±2.4
2@PVDF 9 % (wt %)	6.7±1.5	204±34	7.8±0.5
2@PVDF 50 % (wt %)	2.9±1.1	×	5.6±2.2

UTS: Ultimate tensile strength; E: Elastic Modulus.

a)

PVDF | **1@PVDF** 9 %(wt%) | **1@PVDF** 50 %(wt%) | **2@PVDF** 9 %(wt%) | **2@PVDF** 50 %(wt%)

b)

Figure S21. a) PVDF film and film composites of **1@PVDF** and **2@PVDF** at 9 and 50 wt%. b) **1@PVDF** (9 wt%) during mechanical testing 25 mm wide strip was tested in extension mode at 0.5 mm min^{-1} (left) and sample failure in mechanical testing (right).

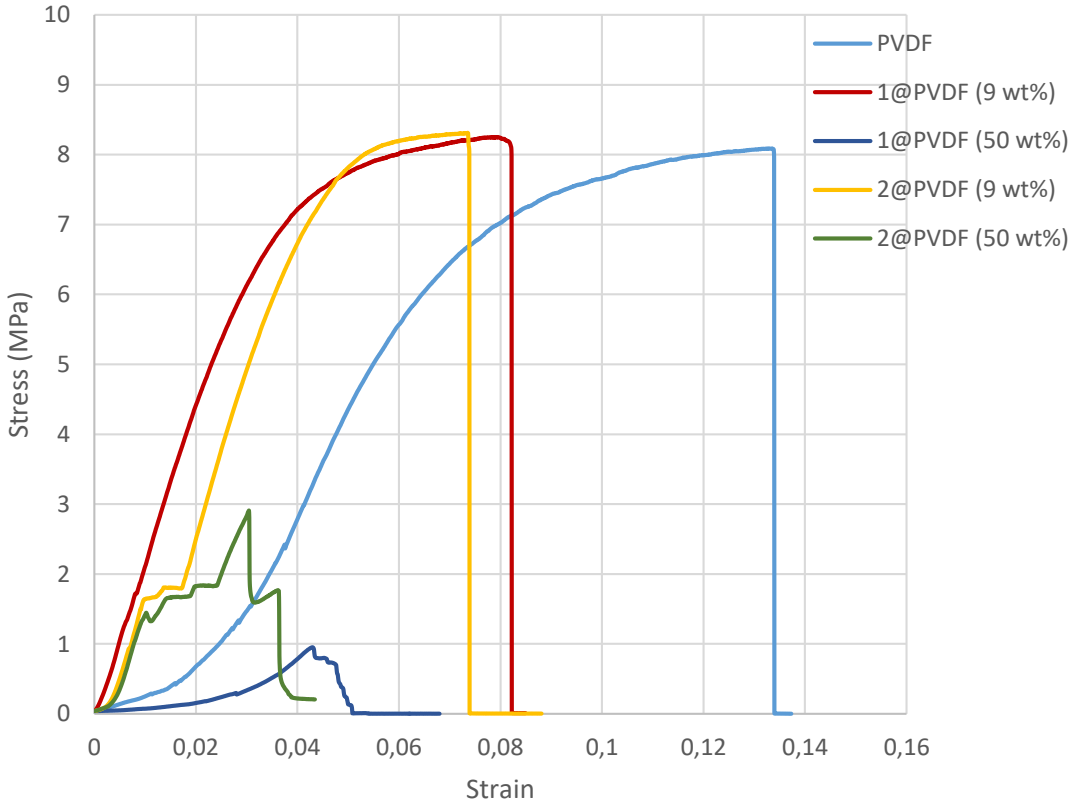

Figure S22. Stress *versus* strain for naked PVDF film and film composites of **1@PVDF** and **2@PVDF** at 9 and 50 wt%. Increasing CP content reduces the strain of the composite, giving a more brittle material.

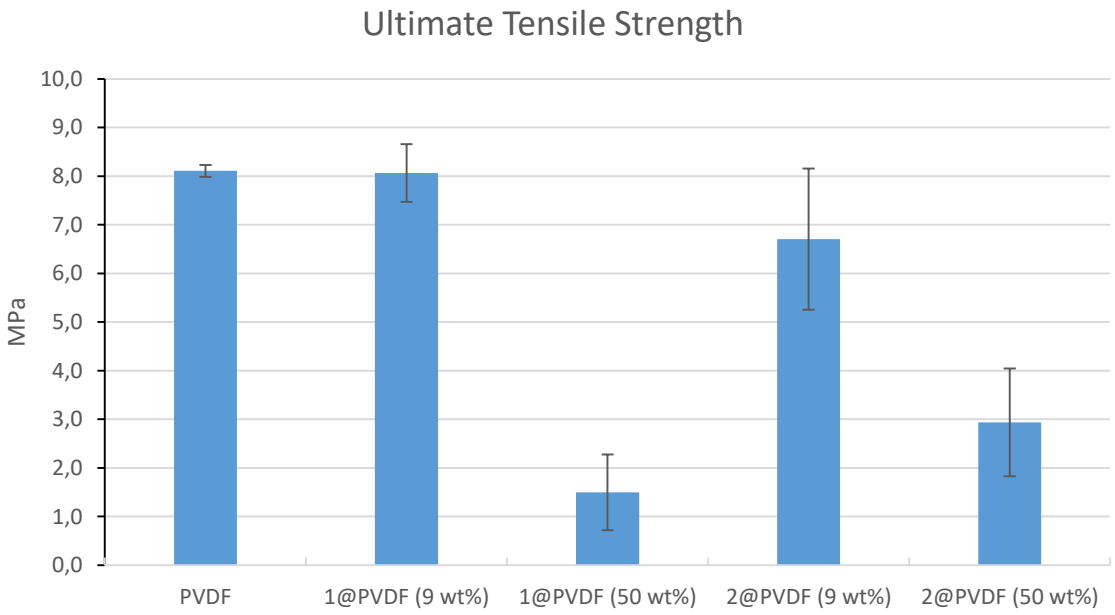

Figure S23. Ultimate tensile strength for naked PVDF film and film composites of **1@PVDF** and **2@PVDF** at 9 and 50 wt%. Increasing CP content to 50 wt% reduces the ultimate tensile strength of the composite while small CP quantities (9 wt%) produces only slight changes.

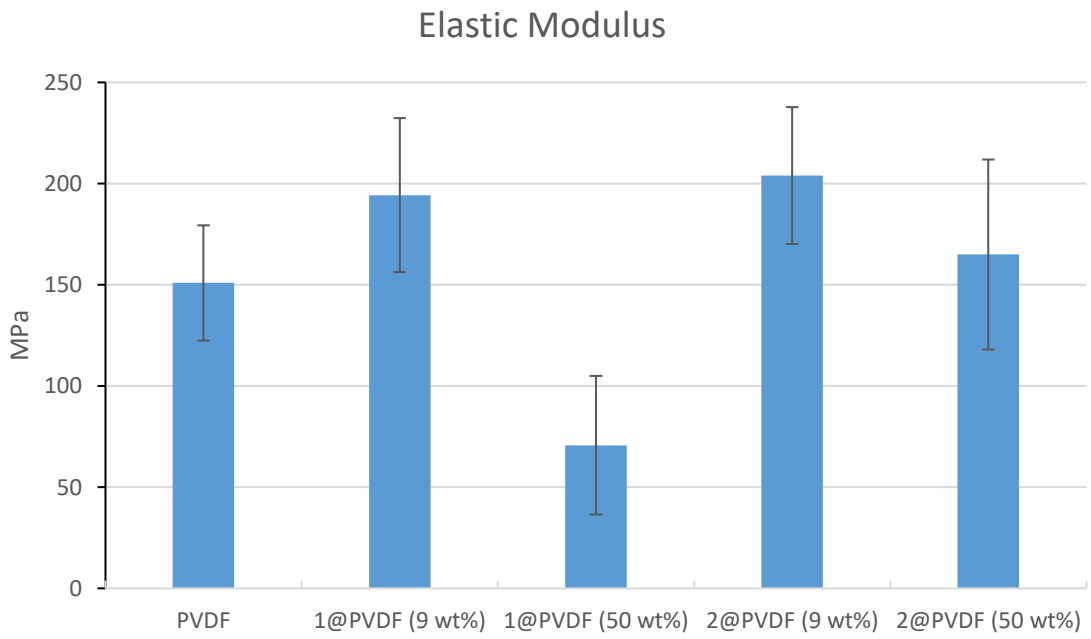

Figure S24. Elastic tensile modulus for naked PVDF film and film composites of **1@PVDF** and **2@PVDF** at 9 and 50 wt%. The increase in elastic modulus with incorporation of 9 wt% CPs is indicative of good adhesion between polymer and CP nanosheets.

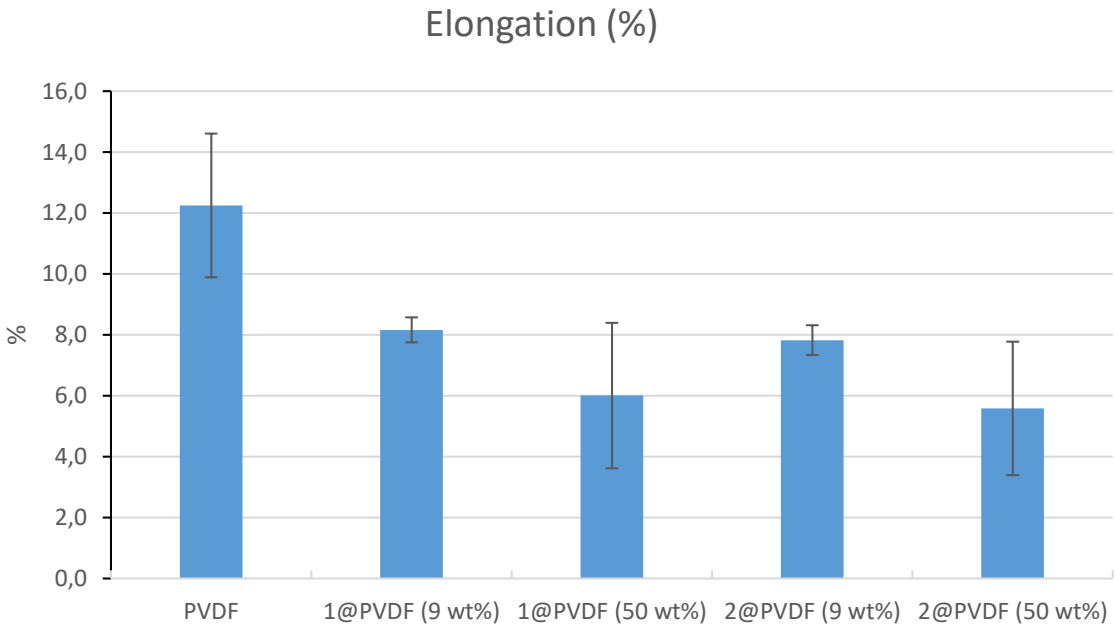

Figure S25. Elongation (%) for naked PVDF film and film composites of **1@PVDF** and **2@PVDF** at 9 and 50 wt %. The reduction in elongation with incorporation of CPs is indicative of the formation of a more brittle material.